URCA SHELLS IN DENSE STELLAR INTERIORS

SACHIKO TSURUTA
Smithsonian Astrophysical Observatory, Cambridge, Mass., U.S.A.

and

A. G. W. CAMERON
Belfer Graduate School of Science, Yeshiva University, New York, N.Y., U.S.A. and Institute for Space Studies, Goddard Space Flight Center, NASA, New York, N.Y., U.S.A.

(Received 27 October, 1969)

Abstract. Thermal and vibrational energy losses due to URCA shells in stellar interiors are calculated. Analytic expressions are derived for semidegenerate, relativistic electrons. Results are given for more general cases calculated with a computer. The calculations are carried out for a large number of nuclei that may contribute to URCA energy losses in various stages of stellar evolution. An illustration is given of the cooling and vibrational damping of a white dwarf. For a central Fermi energy $\gtrsim 5$ MeV, the internal temperature of the star should be reduced to the order of 10^6 K and the relative vibrational amplitude should be reduced to the order of 10^{-5} on a time scale of 10^9 yr. The URCA energy losses are compared with other neutrino energy losses. In a stellar interior where URCA shells are present, the URCA neutrino energy loss dominates in the temperature region up to about 2×10^9 K.

1. Introduction

Conditions of considerable electron degeneracy arise not only in white dwarf stars, which are the end points of evolution of many kinds of stars, but also in many advanced stages of evolution in which stars contain nuclear burning shells. There have been many discussions in the literature of energy losses from these degenerate regions both by thermal conduction and by the plasma process of neutrino-antineutrino emission. In this article, we consider a third kind of energy loss mechanism, that due to the presence of URCA shells.

In the URCA process, a nucleus alternatively captures an electron and undergoes a beta decay, meanwhile emitting a neutrino and an antineutrino. Here we are interested in the electron degenerate case, where the electron Fermi level is in the vicinity of the electron capture threshold. Phase space can be made available for the URCA process either by a thermal rounding of the Fermi surface or by a vibrational oscillation of it.

Only nuclei of odd mass number can participate in the URCA process. There is an odd-even effect in the mass surface, so that after capturing an electron, a nucleus of even mass number has a lowered threshold for capture of a succeeding electron. Hence, only even-mass-number nuclei of even charge number can exist in a degenerate gas, and these will, in general, be stable against both electron capture and beta decay.

A star of roughly solar composition will initially possess 1% or 2% of its mass in the form of heavier elements, beyond helium, but somewhat less than 0.1% of the mass

Astrophysics and Space Science 7 (1970) 374–406.

is in the form of odd-mass-number nuclei. By the time such a star can evolve to a degenerate stage, the interesting nuclei will lie in the range Ne^{21} to Co^{59}. Additional odd-mass-number nuclei can be created by minor reactions associated with helium burning. For example, the CNO bi-cycle will concentrate most initial CNO nuclei as N^{14}. The sequence

$$N^{14}(\alpha, \gamma)\, F^{18}(\beta^+ \nu)\, O^{18}(\alpha, \gamma)\, Ne^{22}(\alpha, n)\, Mg^{25}$$

may then convert something approaching 1% of the mass into Mg^{25}. The neutrons produced will be largely captured by nuclei in the iron peak, moving these nuclei into a higher mass-number range, where about 20% of them will have odd mass numbers.

During carbon burning, substantial amounts of Na^{23}, Mg^{25}, and Al^{27} can be produced. In our illustrative example, we have assumed that such carbon burning has taken place in a stellar core. Arnett (1969) has recently shown that carbon burning should be explosive in most stars, so that our assumption may not be a very good one. However, similar results would have been obtained if we had instead assumed that helium burning had produced substantial quantities of Mg^{25}.

We have thus calculated the thermal and vibrational energy losses from such URCA shells. The nuclear URCA rates without vibration have been treated by Bahcall (1962, 1964), and by Hansen (1966, 1968) and others to a certain extent, and those for matter in nuclear statistical equilibrium have been calculated by Tsuruta and Cameron (Tsuruta, 1964; Tsuruta and Cameron, 1965). However, the present work deals with the combined thermal and vibrational problem in a systematic manner. Simple expressions have been derived and applied to the calculation of total flux from vibrating URCA shells.

In Section 2, basic equations are given. Analytic expressions are derived in Section 3 for semidegenerate, relativistic electrons. In Section 4, more general cases are studied, through the use of an electronic computer, for a wide range of temperatures and vibrational amplitudes that are of interest. The calculations are then extended to a large number of nuclei of odd mass number that might contribute significantly to URCA losses in various stages of stellar evolution. In Section 5, the results are applied to the cooling and vibrational damping of white dwarf stars. Finally, the URCA energy losses are compared with other neutrino energy losses in Section 6.

2. Basic Equations

We consider electron capture and beta decay between a pair of nuclei (Z, A) and $(Z-1, A)$:

$$\begin{aligned} e^- + (Z, A) &\rightarrow (Z-1, A) + \nu, \\ (Z-1, A) &\rightarrow (Z, A) + e^- + \bar{\nu}. \end{aligned} \tag{1}$$

The rates of these reactions and the corresponding neutrino energy losses are found through modification of the theory of ordinary beta reactions as shown in our previous papers (Tsuruta, 1964; Tsuruta and Cameron, 1965; see also Bahcall, 1962, 1964 and

Hansen, 1966, 1968). They can be summarized as follows:

$$\lambda^{+} = \frac{\ln 2}{ft} \int_{W_m}^{\infty} F^{+}(Z, W)\, WP(W - W_m)^2 S\, \mathrm{d}W\,,$$

$$L^{+} = \frac{\ln 2}{ft} \int_{W_m}^{\infty} F^{+}(Z, W)\, WP(W - W_m)^3 S\, \mathrm{d}W\,,$$

$$\lambda^{-} = \frac{\ln 2}{ft} \int_{1}^{W_m} F^{-}(Z, W)\, WP(W_m - W)^2 (1 - S)\, \mathrm{d}W\,, \tag{2}$$

$$L^{-} = \frac{\ln 2}{ft} \int_{1}^{W_m} F^{-}(Z, W)\, WP(W_m - W)^3 (1 - S)\, \mathrm{d}W\,,$$

$$P = \sqrt{W^2 - 1}\,,$$

where

$$S = \{1 + \exp[\beta(W - W_{\mathrm{F}})]\}^{-1} \tag{3}$$

and

$$\beta = m_e c^2 / kT\,.$$

In the above, λ is the reaction rate per nucleus; L is the neutrino energy loss rate per nucleus (in units of electron rest mass, $m_e c^2$); the superscripts + and − denote the electron capture and beta decay, respectively; W is the electron energy, W_m is the electron-capture threshold energy, and W_{F} is the electron Fermi energy, including $m_e c^2$, in units of $m_e c^2$; Z is the charge of the parent nucleus; and T is the temperature.

The factor $F^{\pm}(Z, W)$ takes into account the Coulomb effect, and the factors containing S, the Fermi-Dirac distribution function, take into account all modifications arising from the Pauli exclusion principle. We note that in the URCA process, positron decays may be an alternative to electron capture, but in the dense stellar interiors, which are our primary interest, positron decays are negligible compared to electron captures (Hansen, 1966; Tsuruta, 1964) and hence are not included here.

We now extend our considerations to the URCA process in a star subject to small radial oscillations. Such oscillations can be expressed by the Lagrangian trial function

$$\xi(r, t) = \xi_0(r) \sin \omega t\,. \tag{4}$$

We note that the contribution to the URCA energy losses can come only from a very thin shell with a width determined by an energy spread that is generally much less than the electron Fermi energy. We shall assume that the amplitude $\xi_0(r)$ can be written

$$\xi_0(r) = \mathrm{d}r/r_0 = \text{constant} = \xi_0\,,$$

where $\mathrm{d}r$ is the radial displacement from the equilibrium position r_0. Then,

$$\mathrm{d}r(t) = r_0 \xi_0 \sin \omega t\,. \tag{5}$$

The number density n_e will change about the equilibrium value n_0 as

$$n_e = n_0(1 + \xi_0 \sin \omega t)^{-3} \approx n_0(1 - 3\xi_0 \sin \omega t).$$

The number density and Fermi energy are related by

$$n_e = a_\mu (W_F^2 - 1)^{3/2},$$

where (6)

$$a_\mu = \frac{1}{3\pi^2} \frac{1}{\lambda\!\!\!^{-3}_e}; \quad \lambda\!\!\!^{-}_e = \frac{\hbar}{m_e c}.$$

From these relations, the variation of electron Fermi energy dW_F about the equilibrium value W_{F0} is

$$dW_F = - W_{F0}\xi_0 \sin \omega t. \tag{7}$$

Equations (2) and (3) are also valid for the URCA process in a vibrating star if the W_F in Equation (3) includes the vibration effects

$$W_F = W_{F0} + dW_F = W_{F0}(1 - \xi_0 \sin \omega t) \tag{8}$$

and if the time integrals are averaged over a vibration period.

We are ultimately interested in the total neutrino energy emitted by a star. The contributions to the URCA neutrinos and antineutrinos are negligible outside a thin shell of thermal spread and a spread determined by the vibrational amplitude. Therefore, it is convenient to determine the total neutrino and antineutrino fluxes from such URCA shells. The flux F is

$$\begin{aligned} F &= F^+ + F^- \\ F^\pm &= \int_0^R Q^\pm \, dr \\ Q^\pm &= L^\pm n^\pm, \end{aligned} \tag{9}$$

where $n^\pm$ are the number densities of the parent nuclei, $Q^\pm$ are the URCA energy loss rates per volume, and the superscripts + and − denote the electron capture and beta decay.

The number densities $n^\pm$ are found as follows: Assuming that the matter is entirely made of a pair of participating nuclei (Z, A) and $(Z-1, A)$ whose number densities are n^+ and n^-, we have the relations

$$\begin{aligned} \lambda^+ n^+ &= \lambda^- n^-, \\ n_e &= Z n^+ + (Z - 1)\, n^-. \end{aligned} \tag{10}$$

The first relation satisfies the steady-state condition, and the second states the requirement of charge neutrality. From these equations and Equation (6), we obtain

$$n^\pm = \frac{a_\mu}{Z} (W_F^2 - 1)^{3/2} \frac{\lambda^\mp}{\lambda^+ + \lambda^-}, \tag{11}$$

where the constant a_μ is defined in (6). The result can be easily extended to the case where more than two nuclear species exist in the matter, as shown in Section 4.

The Q is then integrated over the radius (which is the same as integration over the shell) to obtain the flux. However, for practical purposes, it is more convenient to use W_{F0} instead of r as the variable of integration. Then we get

$$F^{\pm} = \frac{a_\mu}{Z}\frac{1}{a_0}\int_{W_{F1}}^{W_{F2}} (W_F^2 - 1)^{3/2}\left(\frac{L^{\pm}\lambda^{\mp}}{\lambda^{+} + \lambda^{-}}\right) dW_{F0}, \tag{12}$$

where W_{F1} and W_{F2} are the values of Fermi energy at the boundaries of the shell where the contribution to the above integral vanishes, and a_0 is the derivative of the Fermi energy with respect to the radius near the shell $|dW_{F0}/dr|$.

3. Analytic Approximations

The exact integration involved in Equations (2) and (3) are too complicated to be handled analytically. However, analytic treatment is possible in the region near $W_F = W_m$, especially if the electrons are near-relativistic (i.e., Fermi energy $E_F = W_F m_e c^2 > m_e c^2$) and semidegenerate ($E_F > kT$). The derivation of such analytic expressions and the study of a rough behavior of the solutions will be both useful and educational, and we devote this section to that purpose.

Using the above conditions and expanding S, the Fermi-Dirac distribution function (Equation (3)), we can carry out the integrations (2). We use the notation

$$\Delta \equiv |W_F - W_m|/W_m$$

and

$$\beta' = \beta W_m = W_m m_e c^2/kT, \tag{13}$$

where Δ is the fractional spread of Fermi energy about the threshold energy, and β'^{-1} measures the thermal width in units of W_m. Since the contributions to the URCA neutrinos and antineutrinos come only from a thin shell near the point $W_m = W_F$, higher order terms in Δ can be neglected, and for semidegenerate matter, higher order terms in β'^{-1} can be neglected, in a first-order approximation. Then, if we retain the lowest order terms in Δ, β'^{-1}, and a coupled term, the integrals reduce to the following expressions:

Region (I): $W_F \gtrsim W_m$

$$\begin{aligned}
\lambda_I^{+} &= C^{+} W_m^5 \left[\frac{\Delta^3}{3} + \frac{2}{\beta'^3}\exp(-\beta'\Delta) + \frac{1}{\beta'^2} f_1(\Delta)\right], \\
L_I^{+} &= C^{+} W_m^6 \left\{\frac{\Delta^4}{4} + \frac{1}{\beta'^4}[f_3(\Delta) - 6\exp(-\beta'\Delta)] + \frac{1}{\beta'^2} f_2(\Delta)\right\}, \\
\lambda_I^{-} &= C^{-} W_m^5 \frac{2}{\beta'^3}\exp(-\beta'\Delta), \\
L_I^{-} &= C^{-} W_m^6 \frac{6}{\beta'^4}\exp(-\beta'\Delta).
\end{aligned} \tag{14}$$

Region (II): $W_F \lesssim W_m$

$$\lambda_{II}^{+} = \left(\frac{C^{+}}{C^{-}}\right)\lambda_{I}^{-}, \quad L_{II}^{+} = \left(\frac{C^{+}}{C^{-}}\right)L_{I}^{-},$$
$$\lambda_{II}^{-} = \left(\frac{C^{-}}{C^{+}}\right)\lambda_{I}^{+}, \quad L_{II}^{-} = \left(\frac{C^{-}}{C^{+}}\right)L_{I}^{+}, \tag{15}$$

where

$$C^{\pm} = \left(\frac{\ln 2}{ft}\right)\langle F\rangle^{\pm},$$
$$\langle F\rangle^{\pm} = \frac{2\pi\bar{\eta}}{|1 - \exp(\mp 2\pi\bar{\eta})|}, \tag{16}$$
$$\bar{\eta} = \alpha Z\left\langle\frac{\bar{W}}{P}\right\rangle = \alpha Z\left(\frac{W_m}{P_m}\right),$$
$$P_m = (W_m^2 - 1)^{1/2},$$

and

$$f_1(\Delta) = 4(2\Delta - 1)(\Delta + 1)\Delta,$$
$$f_2(\Delta) = 2(5\Delta + 3)(\Delta + 1)\Delta^2, \tag{17}$$
$$f_3(\Delta) = 12(10\Delta^2 + 8\Delta + 1).$$

In the above, Z is the charge of the parent nucleus, and $\alpha = \frac{1}{137}$. The details of the derivation of the above results are given in Appendix 1.

We note from Equation (17) that as $\Delta \to 0$,

$$f_1(\Delta) \to 0, \quad f_2(\Delta) \to 0, \quad \text{and} \quad f_3(\Delta) \to 12,$$

and from Equations (14) and (15) that

$$\left.\begin{aligned}\lambda^{\pm} &\to a_{\lambda}^{\pm}\Delta^3\\ L^{\pm} &\to a_{L}^{\pm}\Delta^4\end{aligned}\right\} \quad \text{as} \quad T \to 0,$$

and

$$\left.\begin{aligned}\lambda^{\pm} &\to b_{\lambda}^{\pm}T^3\\ L^{\pm} &\to b_{L}^{\pm}T^4\end{aligned}\right\} \quad \text{as} \quad \Delta \to 0,$$

and we can roughly write

$$\lambda^{\pm} \approx a_{\lambda}^{\pm}\Delta^3 + b_{\lambda}^{\pm}T^3$$
and (18)
$$L^{\pm} \approx a_{L}^{\pm}\Delta^4 + b_{L}^{\pm}T^4.$$

In the above equations, $\Delta = 0$ for electron captures if $W_F \leqslant W_m$, and $\Delta = 0$ for beta decays if $W_F \geqslant W_m$. The constants of proportionality appearing in Equation (18) are

$$a_{\lambda}^{\pm} = C^{\pm}W_m^5/3, \quad a_{L}^{\pm} = C^{\pm}W_m^6/4;$$
$$b_{\lambda}^{\pm} = C^{\pm}W_m^2 2\left(\frac{k}{m_e c^2}\right)^3, \quad b_{L}^{\pm} = C^{\pm}W_m^2 6\left(\frac{k}{m_e c^2}\right)^4. \tag{19}$$

The URCA rates for vibration are obtained by use of the expression for W_F as given in Equation (8). Rough analytic expressions (before the time integration) are then (see Appendix 2)

$$\begin{aligned} \lambda &= a_\lambda(\Delta_0 + \delta)^3 + b_\lambda T^3, \\ L &= a_L(\Delta_0 + \delta)^4 + b_L T^4, \end{aligned} \tag{20}$$

where

$$\begin{aligned} \Delta_0 &= |W_{F0} - W_m|/W_m, \\ \delta &= \mathrm{d}W_F/W_m = -u_0'\xi_0 \sin\omega t, \\ u_0' &= W_{F0}/W_m. \end{aligned} \tag{21}$$

That is, δ is the fractional change of Fermi level due to vibration, Δ_0 and u_0' are Δ and u' at the equilibrium point r_0, u' is the electron Fermi energy in units of W_m, and ξ_0 is the vibrational amplitude at the point of maximum expansion and maximum compression. The above general expressions apply to both electron captures and beta decays if appropriate values are used for the constants of proportionality a_i and b_i ($i=\lambda, L$). When $W_{F0}=W_m$, we have $\Delta_0=0$. In this case, electron captures take place during compression periods and beta decays take place during expansion periods (neglecting thermal effects).

After time integrations are carried out, the total rates can be expressed as follows (see Appendix 2):

$$\begin{aligned} \lambda &= a_\lambda \sum_{n=0}^{3} a_n' \Delta_0^{3-n} u_0'^n \xi_0^n + b_\lambda T^3, \\ L &= a_L \sum_{n=0}^{4} b_n' \Delta_0^{4-n} u_0'^n \xi_0^n + b_L T^4, \end{aligned} \tag{22}$$

where a_n' and b_n' are constants and are given in Appendix 2 (Equation A31).

Near the threshold point $W_{F0}=W_m$ (that is, $\Delta_0=0$), the above equations reduce to (Appendix 2)

$$\begin{aligned} \lambda &= \left(\frac{2}{3\pi} a_\lambda u_0'^3\right) \xi_0^3 + b_\lambda T^3, \\ L &= \left(\frac{3}{16} a_L u_0'^4\right) \xi_0^4 + b_L T^4. \end{aligned} \tag{23}$$

That is, the beta reaction rates depend on the third powers of amplitude and temperature, and the corresponding energy loss rates depend on the fourth powers of amplitude and temperature.

We can proceed similarly to obtain the flux F. However, the situation is more complicated because it includes the product of $L^{\pm}$ and $\lambda^{\mp}$ (the product of the electron-capture and beta-decay terms), which has to be integrated over the Fermi energy (see Equation (12)). After lengthy calculations, as shown in Appendix 3, we obtain the following approximate expression for the relativistic case ($W_m \gg 1$):

$$F = 6\left(\frac{\ln 2}{ft}\right)\left(\frac{a_\mu}{a_0 Z}\right)\left(\frac{\langle F\rangle^+\langle F\rangle^-}{\langle F\rangle^+ + \langle F\rangle^-}\right) W_m^{10}\left[\frac{1}{64\pi}\xi_0^5 + 4\left(\frac{k}{W_m m_e c^2}\right)^5 T^5\right], \tag{24}$$

in units of $m_e c^2/\text{cm}^2$ sec. That is, the flux depends roughly on the fifth powers of amplitude and temperature.

In the above derivations, the approximation $P=\sqrt{(W^2-1)}=W$ has been made. Analytic considerations for a more general case without this approximation are discussed in Appendix 4.

4. Exact Solutions – Computer Results

To show the behavior of the exact solutions, we carried out the integrations of (2) and (3) on the CDC 6400 computer for sample cases of $W_m=1.5$, 10, 20, and 40 (which cover the threshold energy of up to about 20 MeV) with $Z=10$. The temperatures range from $\sim 10^3$ K to 10^{10} K, and the amplitudes ξ_0 and the widths Δ_0 covered are from ~ 0.1 to zero. In these calculations, the Coulomb factor $F^{\pm}(Z, W)$ was retained in the integrals and we used the expression (Feenberg and Trigg, 1950)

$$F^{\pm}(Z, W)=\frac{2\pi\eta}{|1-\exp(\mp 2\pi\eta)|}, \quad \eta=\alpha Z(W/P). \tag{25}$$

That is, the term W/P in η was not replaced by the threshold value of W_m/P_m (the approximation used in Section 3). We set $\log ft=5.5$, which should be adequate for the present investigation.

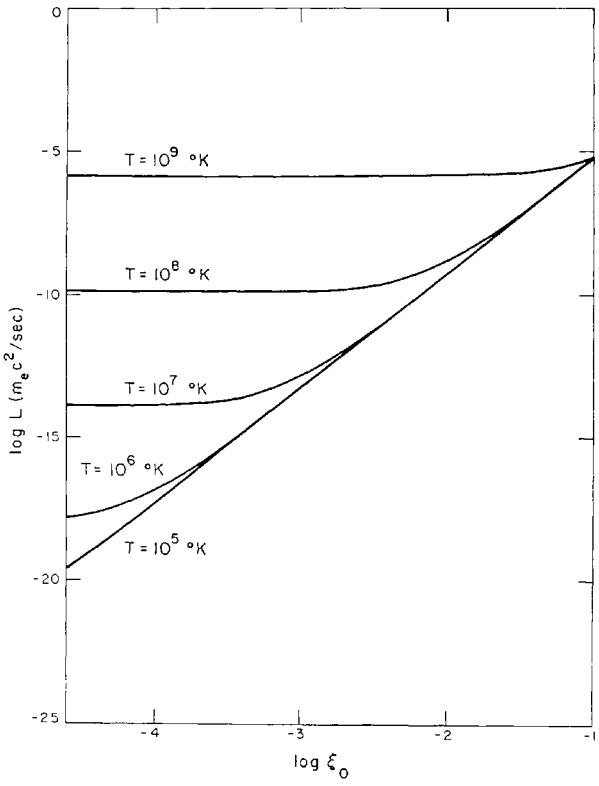

Fig. 1. URCA neutrino energy loss rates per nucleus as a function of temperature T and amplitude ξ_0 for electron captures when the width of the equilibrium point $\Delta_0=0$.

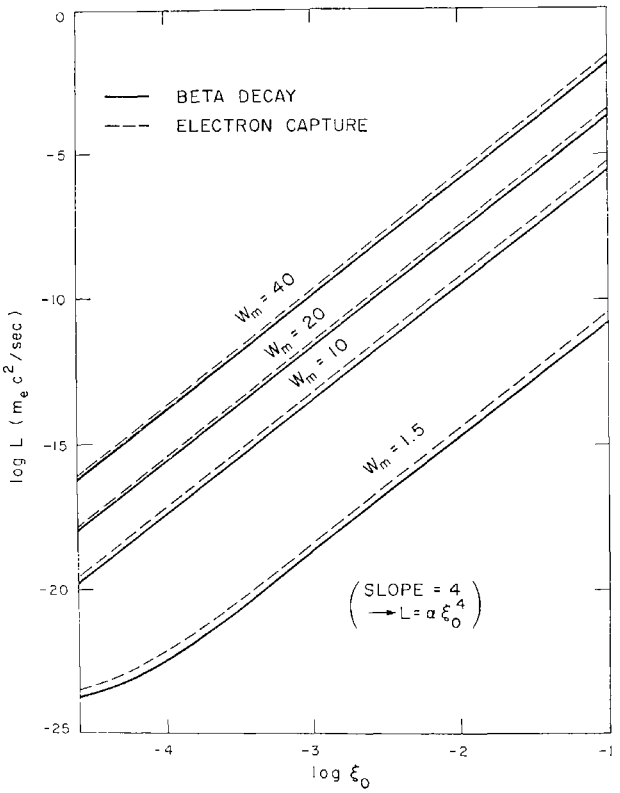

Fig. 2. Amplitude dependence of URCA neutrino energy loss rates per nucleus for electron captures and beta decays at $T = 10^5$ K and $\Delta_0 = 0$ for a family of values of electron threshold energy W_m.

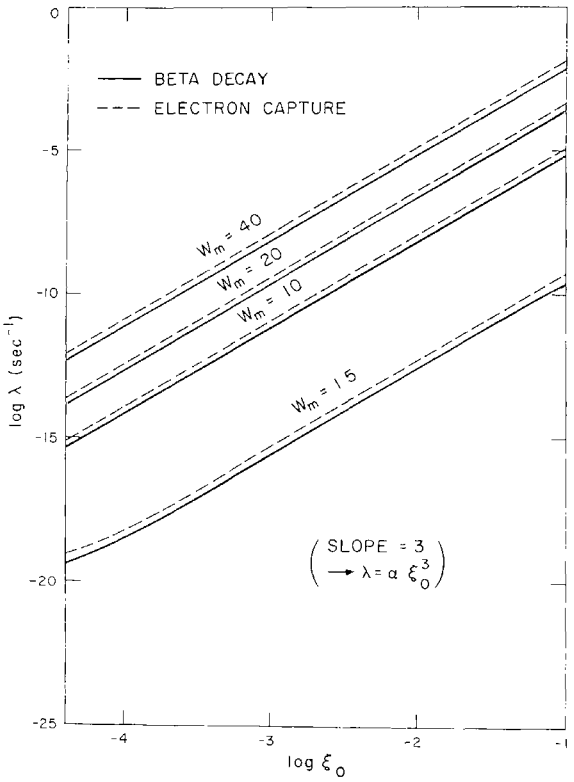

Fig. 3. Amplitude dependence of URCA reaction rates per nucleus for electron captures and beta decays at $T = 10^5$ K and $\Delta_0 = 0$ for various values of W_m.

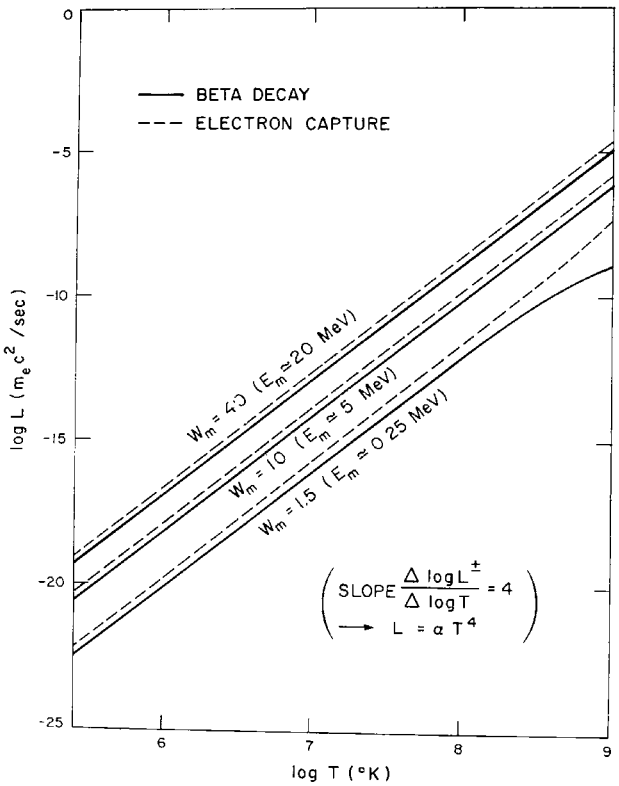

Fig. 4. Temperature dependence of URCA neutrino energy loss rates per nucleus for electron captures and beta decays at $\xi_0 = 0$ and $\Delta_0 = 0$ for various values of W_m.

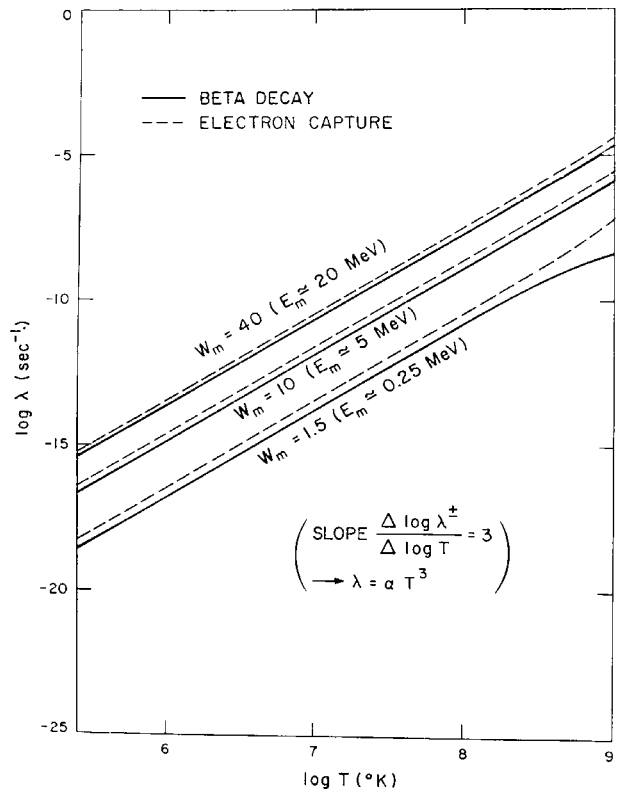

Fig. 5. Temperature dependence of URCA reaction rates per nucleus for electron captures and beta decays at $\xi_0 = 0$ and $\Delta_0 = 0$ for various values of W_m.

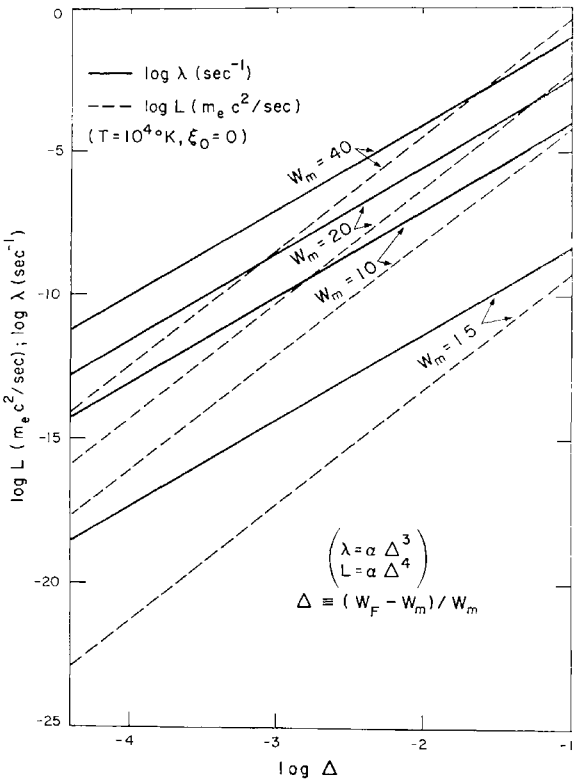

Fig. 6. URCA reaction rates λ and energy loss rates L as a function of the width Δ defined as $\Delta = (W_F - W_m)/W_m$ for electron captures at $T = 10^4$ K and $\xi_0 = 0$ for various values of W_m.

The results are summarized in Figures 1 to 6. In Figure 1, the behavior of L as a function of T and ξ_0 is shown at the point $W_m = W_{F0} = 10$. We note that for sufficiently low temperatures, the $\log L$ vs $\log \xi_0$ curves approach a straight line. Similar curves are shown for several values of W_m in Figure 2. A low-temperature value of 10^5 K was used to show the effect of amplitude. These curves indicate that the vibrational component of L goes as ξ_0^4. Similarly, Figure 3 shows that the vibrational term of λ goes as ξ_0^3. The temperature effect on L and λ is shown in Figures 4 and 5, where ξ_0 and Δ_0 were set equal to zero to eliminate other terms. We note that the thermal terms in L and λ go as T^4 and T^3, respectively. Finally, Figure 6 shows the dependence of L and λ on Δ.

We conclude that the simple expressions of Equations (18) and (23) derived through analytic approximations are still valid in the exact solutions, in most of the ranges of interest, if suitable values are given for the proportionality constants a_i and b_i ($i = \lambda$ or L). For relativistic degenerate electrons, these constants are given by the simple forms of (19). Without such approximations, the exact expressions are more complicated, involving momentum P_m as well as energy W_m (as discussed in Appendix 4). However, the L's and λ's still depend on the third and the fourth powers of temperature and width (including vibration), respectively. Therefore, the correct values of a_i and b_i in (18) are easily calculated through the help of a computer for any pair of nuclei of interest.

We note some deviation from the slopes of 3 and 4 for λ and L for the $W_m = 1.5$ case when the amplitude ξ_0 is less than about 10^{-4} (Figures 2 and 3), but this disappears when the temperature becomes sufficiently low ($\lesssim 10^4$ K). The thermal terms show (Figures 4 and 5) some appreciable deviation (from the slopes of 4 and 3) for low values of W_m and very high temperatures (near 10^9 K). This is expected from physical considerations. We note that the general agreement with our analytic work is excellent.

Similar investigations were made for the behavior of flux using the same ranges of temperature and amplitude. For this purpose, we chose five pairs of nuclei that may be of particular interest, which are shown in Table I. These were selected to cover a

TABLE I

Properties of the nuclear pairs chosen for our studies of URCA flux

URCA nuclear pair	Threshold energy (Mev)	log*ft*
(1) $Cl^{35} \rightleftarrows S^{35}$	0.168	5.0
(2) $P^{31} \rightleftarrows Si^{31}$	1.48	5.5
(3) $Na^{23} \rightleftarrows Ne^{23}$	4.4	5.3
(4) $Ne^{23} \rightleftarrows F^{23}$	11.15	5.5
(5) $O^{23} \rightleftarrows N^{23}$	23.33	8.0

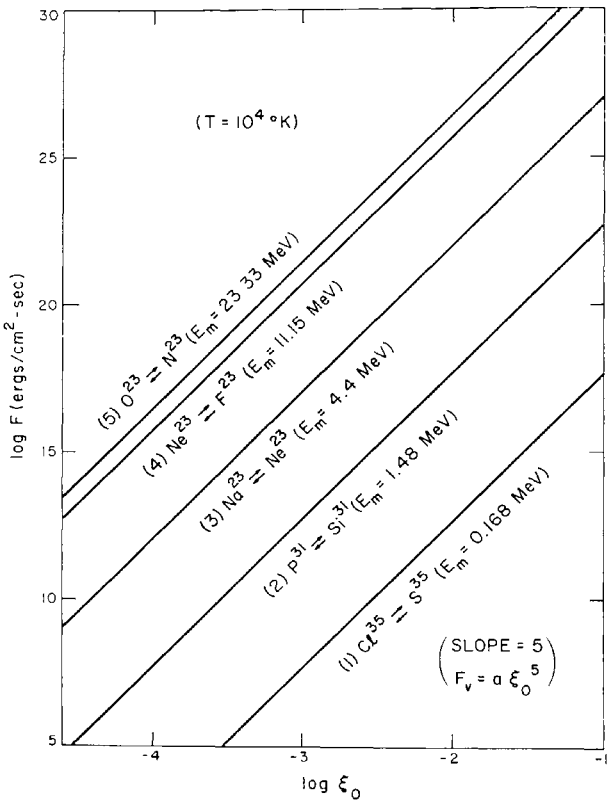

Fig. 7. Amplitude dependence of total neutrino flux from vibrating URCA shells for the five nuclear pairs as shown.

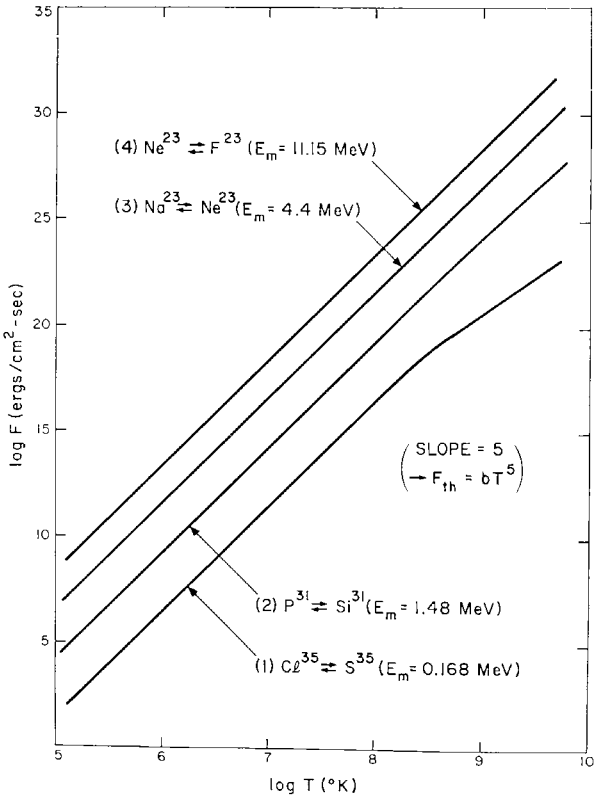

Fig. 8. Temperature dependence of total neutrino flux from URCA shells for the four nuclear pairs as shown.

sufficiently wide range of threshold energy, from near zero to about 23 MeV. The *ft* values used for each case are also shown in Table I. The integrals (12) have been carried out for these five cases, and the results are shown in Figures 7 and 8. For the value of a_0 appearing in (12), we used the following:

$$\left|\frac{dE_F}{dr}\right| = a_0 m_e c^2 = 4 \times 10^{-8} \text{ MeV/cm}.$$

This represents a typical value for massive white dwarfs (see Section 5, where a_0 for our particular white dwarf model is calculated). The amplitude dependence of $F \propto \xi_0^5$ is apparent in Figure 7, where temperature is set at a sufficiently low value of 10^4 K. Similarly, Figure 8 shows that the thermal component of F goes as T^5 (here, amplitude is set to 0). Thus, most generally we can express flux in a simple form

$$F = a\xi_0^5 + bT^5. \tag{26}$$

This result agrees with Equation (24), which was obtained through crude analytic approximations. However, the constants of proportionality a and b above are generally much more complicated than the simple expression (24) implies. Here again, a computer must be used to evaluate a and b. We obtain a by calculating the value of F at a given amplitude ξ_0 with a sufficiently low temperature. Similarly, b is obtained by calculating F at a given T, setting $\xi_0 = 0$.

Figures 7 and 8 indicate that the deviation from the simple expression of (26) is appreciable only in the very high-temperature region ($T \gtrsim 10^9$ K) of a nuclear pair with an extremely low threshold energy, as in the case (1) with 0.168 MeV. Since most of the nuclear pairs of interest do not have such low threshold energies, we may well neglect this small deviation in the subsequent calculations.

When we are interested only in crude estimates of URCA energy losses or when electrons are relativistic and degenerate, the analytic equations derived in Section 3 may be sufficient. For more quantitative studies of more general cases, the computer method outlined above is desirable. At this point, we can note that the flux in (12) has been derived for matter consisting of a pair of nuclei (Z, A) and $(Z-1, A)$. For a more general case, when other nuclei are also present, this flux has to be multiplied by the factor χ defined as (see Appendix 5 for the derivation)

$$\chi = \chi_i(\bar{\mu}_e/\mu_e), \quad \chi_i = \varrho_i/\varrho,$$
$$\mu_e = \frac{A_i}{Z_i}, \quad \text{and} \quad \bar{\mu}_e \equiv \left(\sum_{j=1}^{m} \chi_j \frac{Z_j}{A_j}\right)^{-1} = \left\langle \frac{\bar{A}}{\bar{Z}} \right\rangle. \tag{27}$$

Here, Z_i and A_i are the charge and mass number, and χ_i is the mass fraction, of the pair of URCA nuclei in question; and $\bar{\mu}_e$ is the average value of A/Z of the medium. Noting that μ_e and $\bar{\mu}_e$ are roughly the same in most cases, we can say that χ is approximately the mass fraction of the URCA nuclei. We also note that a_0 is generally different in different problems. Thus, it will be more convenient if we rewrite Equation (26) as

$$F = \chi \left(\left|\frac{dE_F}{dr}\right|\right)^{-1} (F_1 \xi_0^5 + F_2 T^5), \tag{28}$$

and then find F_1 and F_2 of each pair of nuclei (of interest), using a computer. We note that F_1 and F_2 are characteristic of a given pair of URCA nuclei, determined by its ft value, threshold energy, and charge. We have thus calculated F_1 and F_2 for a total of 132 nuclear pairs that may be of interest in various possible applications in later stages of stellar evolution. These are nuclei with mass numbers ranging from 13 to 61, with threshold energies going up to about 25 MeV. These threshold energies extend beyond those likely to be of interest under hydrostatically stable conditions. Hydrodynamic collapse of stellar cores is likely to commence by at least a Fermi energy of 15 MeV. However, this collapse may possibly proceed very slowly in its initial stages, and the URCA energy loss rates may still be of interest at somewhat higher densities. Thus, we decided to include those electron captures in the relevant mass-number range up to capture thresholds of about 25 MeV.

The results are shown in Table II. The units of F_1 and F_2 are such that $|dE_F/dr| = a_0 m_e c^2$ is expressed in MeV/cm, T in K, and the flux F in ergs/cm^2 sec. In Tables I and II, we took the ft values from latest experimental data where possible; otherwise, we estimated them by making shell-model assignments of ground-state spins and parities

TABLE II

Characteristic properties of URCA nuclear pairs. F_1 and F_2 are defined by Equation (28). The units of F_1 and F_2 are such as to give the flux F in units of ergs/cm^2 sec while dE_F/dr is expressed in MeV/cm

Nuclear pair	Threshold energy (MeV)	$\log F_1$ (ergs MeV/ cm^3 sec)	$\log F_2$ (ergs MeV/ cm^3 sec K^5)	$\log ft$
$N^{15} \rightleftarrows C^{15}$	9.77	27.3208	−24.7610	6.1
C^{13} B^{13}	13.4	30.3023	−22.4356	4.5
O^{17} N^{17}	8.67	24.8699	−26.9661	8.0
N^{17} C^{17}	14.59	27.0909	−25.8247	8.0
C^{17} B^{17}	26.71	29.7176	−24.4768	8.0
F^{19} O^{19}	4.81	25.0443	−25.6092	5.4
O^{19} N^{19}	14.07	26.8796	−25.9595	8.0
N^{19} C^{19}	20.57	28.5397	−25.0997	8.0
Ne^{21} F^{21}	5.7	25.5707	−25.4172	5.5
F^{21} O^{21}	10.90	28.2623	−24.0446	5.5
O^{21} N^{21}	19.43	28.2391	−25.2791	8.0
N^{21} C^{21}	23.54	29.1120	−24.8133	8.0
Na^{23} Ne^{23}	4.4	24.7046	−25.7740	5.3
Ne^{23} F^{23}	11.15	28.3093	−24.0440	5.5
F^{23} O^{23}	13.87	29.2671	−23.5414	5.5
O^{23} N^{23}	23.33	29.0148	−24.8910	8.0
Mg^{25} Na^{25}	3.76	24.1556	−26.0199	5.2
Na^{25} Ne^{25}	7.27	20.0081	−31.4675	12.0
Ne^{25} F^{25}	15.05	23.0625	−29.9166	12.0
F^{25} O^{25}	26.46	31.9981	−22.1749	5.5
Al^{27} Mg^{27}	2.62	15.9582	−33.5438	12.0
Mg^{27} Na^{27}	8.05	20.3840	−31.2980	12.0
Na^{27} Ne^{27}	10.96	28.1949	−24.1221	5.5
Ne^{27} F^{27}	18.19	30.3607	−23.0171	5.5
F^{27} O^{27}	20.96	31.0077	−22.6704	5.5
Si^{29} Al^{29}	3.7	17.2229	−32.9203	12.0
Al^{29} Mg^{29}	6.36	25.8911	−25.3136	5.5
Mg^{29} Na^{29}	10.79	28.0906	−24.1934	5.5
Na^{29} Ne^{29}	14.37	29.3254	−23.5560	5.5
Ne^{29} F^{29}	21.59	31.0861	−22.6541	5.5
P^{31} Si^{31}	1.48	20.3797	−28.1367	5.5
Si^{31} Al^{31}	6.88	26.1742	−25.1877	5.5
Al^{31} Mg^{31}	9.76	27.6387	−24.4372	5.5
Mg^{31} Na^{31}	14.20	29.2360	−23.6198	5.5
Na^{31} Ne^{31}	18.84	27.9661	−25.4851	8.0
Ne^{31} F^{31}	25.73	29.3317	−24.7811	8.0
S^{33} P^{33}	0.25	16.0769	−30.3410	5.0
P^{33} Si^{33}	4.91	24.7928	−25.8966	5.5
Si^{33} Al^{33}	10.29	27.8231	−24.3610	5.5
Al^{33} Mg^{33}	14.23	26.7082	−26.1512	8.0
Mg^{33} Na^{33}	18.34	27.8129	−25.5808	8.0
Na^{33} Ne^{33}	21.02	28.4297	−25.2532	8.0
Cl^{35} S^{35}	0.168	15.2852	−30.8809	5.0
S^{35} P^{35}	3.68	23.6396	−26.4915	5.5
P^{35} Si^{35}	9.38	16.9086	−35.0839	16.0
Si^{35} Al^{35}	14.42	26.7297	−26.1568	8.0
Al^{35} Mg^{35}	16.43	27.3124	−25.8489	8.0

Table II (Continued)

Nuclear pair	Threshold energy (MeV)	$\log F_1$ (ergs MeV/ cm^3 sec)	$\log F_2$ (ergs MeV/ cm^3 sec K^5)	$\log ft$
$Mg^{35} \rightleftarrows Na^{35}$	20.56	28.2964	−25.3389	8.0
Cl^{37} S^{37}	4.80	22.8444	−27.7987	7.3
S^{37} P^{37}	7.82	16.1323	−35.4872	16.0
P^{37} Si^{37}	11.57	17.7776	−34.6486	16.0
Si^{37} Al^{37}	16.65	27.3342	−25.8542	8.0
Al^{37} Mg^{37}	18.70	27.8584	−25.5756	8.0
Mg^{37} Na^{37}	22.88	28.7500	−25.1120	8.0
K^{39} Ar^{39}	0.57	13.0036	−34.1763	9.9
Ar^{39} Cl^{39}	3.43	21.0145	−28.9813	7.8
Cl^{39} S^{39}	6.88	23.5830	−27.7761	8.0
S^{39} P^{39}	10.05	17.1631	−34.9706	16.0
P^{39} Si^{39}	13.85	18.5285	−34.2726	16.0
Si^{39} Al^{39}	18.95	27.8804	−25.5808	8.0
K^{41} Ar^{41}	2.49	18.9921	−30.4119	8.6
Ar^{41} Cl^{41}	5.65	22.7636	−28.2000	8.0
Cl^{41} S^{41}	9.15	24.7473	−27.1923	8.0
S^{41} P^{41}	12.37	18.0258	−34.5385	16.0
P^{41} Si^{41}	15.79	19.0788	−33.9972	16.0
Si^{41} Al^{41}	20.82	28.2788	−25.3815	8.0
Ca^{43} K^{43}	1.82	16.4476	−32.4065	10.0
K^{43} Ar^{43}	4.77	22.0661	−28.5625	8.0
Ar^{43} Cl^{43}	7.97	24.1537	−27.5024	8.0
Cl^{43} S^{43}	11.10	25.5461	−26.7921	8.0
S^{43} P^{43}	14.22	18.6087	−34.2467	16.0
P^{43} Si^{43}	18.88	27.8327	−25.6199	8.0
Sc^{45} Ca^{45}	0.25	14.9352	−31.4739	6.0
Ca^{45} K^{45}	4.19	21.5336	−28.8419	8.0
K^{45} Ar^{45}	6.71	23.4282	−27.8782	8.0
Ar^{45} Cl^{45}	9.84	25.0197	−27.0684	8.0
Cl^{45} S^{45}	14.17	26.5652	−26.2818	8.0
S^{45} P^{45}	18.20	27.6473	−25.7268	8.0
Ti^{47} Sc^{47}	0.60	16.8649	−30.3705	6.1
Sc^{47} Ca^{47}	1.98	18.2188	−30.7784	8.5
Ca^{47} K^{47}	6.05	22.9860	−28.1115	8.0
K^{47} Ar^{47}	9.80	24.9767	−27.1019	8.0
Ar^{47} Cl^{47}	13.80	26.4269	−26.3636	8.0
Cl^{47} S^{47}	17.08	27.3505	−25.8887	8.0
Ti^{49} Sc^{49}	2.01	21.0485	−27.9734	5.7
Sc^{49} Ca^{49}	5.2	18.3578	−32.4379	12.0
Ca^{49} K^{49}	10.03	25.0474	−27.0778	8.0
K^{49} Ar^{49}	12.70	26.0533	−26.5626	8.0
Ar^{49} Cl^{49}	16.26	27.1158	−26.0188	8.0
Cl^{49} S^{49}	19.51	27.9124	−25.6075	8.0
V^{51} Ti^{51}	2.46	15.4523	−33.9248	12.0
Ti^{51} Sc^{51}	6.22	19.0498	−32.1006	12.0
Sc^{51} Ca^{51}	8.13	20.1595	−31.5336	12.0
Ca^{51} K^{51}	12.49	25.9586	−26.6214	8.0
K^{51} Ar^{51}	15.13	26.7867	−26.1955	8.0
Ar^{51} Cl^{51}	18.48	26.6557	−25.7486	8.0

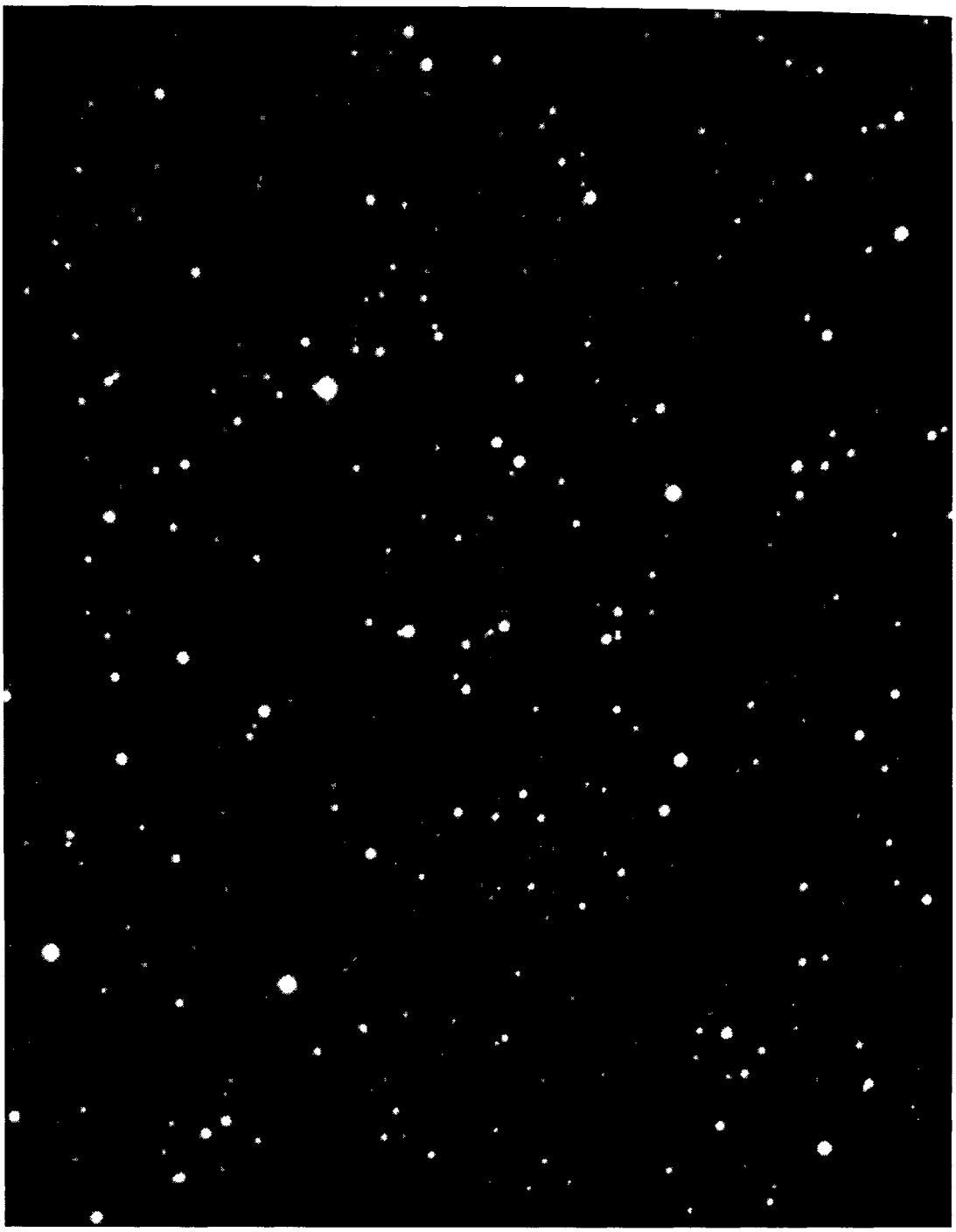

Planetary nebula NGC 6337 ($\alpha = 17h\ 18.8$ min; $\delta = -38°\ 2'$; 1950.0), discovered by John Herschel in 1834, and photographed with the 60-inch Rockefeller reflector of the Boyden Station of Harvard Observatory at Bloemfontein, South Africa (East on top; North to the right).

Table II (Continued)

Nuclear pair	Threshold energy (MeV)	$\log F_1$ (ergs MeV/ cm^3 sec)	$\log F_2$ (ergs MeV/ cm^3 sec K^5)	$\log ft$
$Cl^{51} \rightleftarrows S^{51}$	21.80	28.3827	−25.3722	8.0
Cr^{53} V^{53}	3.54	16.7914	−33.2565	12.0
V^{53} Ti^{53}	5.39	18.4544	−32.4096	12.0
Ti^{53} Sc^{53}	8.68	20.4043	−31.4212	12.0
Sc^{53} Ca^{53}	10.55	21.2324	−30.9959	12.0
Ca^{53} K^{53}	14.71	26.6434	−26.2786	8.0
K^{53} Ar^{53}	17.42	27.3801	−25.8985	8.0
Ar^{53} Cl^{53}	20.49	28.0926	−25.5300	8.0
Mn^{55} Cr^{55}	2.50	22.2679	−27.1353	5.2
Cr^{55} V^{55}	5.66	18.6273	−32.3322	12.0
V^{55} Ti^{55}	7.82	19.9547	−31.6566	12.0
Ti^{55} Sc^{55}	10.90	21.3444	−30.9502	12.0
Sc^{55} Ca^{55}	12.85	28.5531	−24.0850	5.5
Ca^{55} K^{55}	16.72	27.1820	−26.0090	8.0
K^{55} Ar^{55}	19.58	27.8740	−25.6514	8.0
Fe^{57} Mn^{57}	2.70	15.7303	−33.8109	12.0
Mn^{57} Cr^{57}	5.10	24.6917	−26.0603	5.5
Cr^{57} V^{57}	7.87	19.9589	−31.6640	12.0
V^{57} Ti^{57}	10.12	27.5143	−24.6255	5.5
Ti^{57} Sc^{57}	12.90	28.5460	−24.0989	5.5
Sc^{57} Ca^{57}	15.02	29.2068	−23.7577	5.5
Ca^{57} K^{57}	18.71	27.6567	−25.7715	8.0
Co^{59} Fe^{59}	1.56	14.8629	−33.7236	10.9
Fe^{59} Mn^{59}	4.69	24.3403	−26.2458	5.5
Mn^{59} Cr^{59}	7.39	26.1812	−25.3124	5.5
Cr^{59} V^{59}	9.88	27.3932	−24.6957	5.5
V^{59} Ti^{59}	12.28	28.3178	−24.2231	5.5
Ti^{59} Sc^{59}	14.90	29.1497	−23.7966	5.5
Sc^{59} Ca^{59}	17.11	29.7551	−23.4833	5.5
Ni^{61} Co^{61}	1.29	13.1112	−35.1690	12.0
Co^{61} Fe^{61}	3.92	23.6209	−26.6165	5.5
Fe^{61} Mn^{61}	6.69	25.7570	−25.5340	5.5
Mn^{61} Cr^{61}	9.55	27.2317	−24.7858	5.5
Cr^{61} V^{61}	11.88	28.1579	−24.3127	5.5
V^{61} Ti^{61}	14.36	28.9723	−23.8954	5.5
Ti^{61} Sc^{61}	16.93	29.6871	−23.5277	5.5

and assigning typical values of $\log ft$ depending on the degree of forbiddenness. The electron-capture threshold energies have been taken from experimental data where available, and otherwise from Garvey and Kelson (1966).

5. Application to Some Observational Aspects of White Dwarfs

URCA neutrinos can play an important role in white dwarfs that are massive enough, and hence dense enough, to contain URCA shells. In order to study an example of neutrino and antineutrino emission from such stars, a white dwarf model was chosen

that is stable but near the maximum mass point. The model was constructed in hydrostatic equilibrium, with pressure due to electron degeneracy. However, general relativistic hydrostatic equations were used, and the change of composition due to electron capture in higher density regions was taken into account. We assumed that carbon burning had occurred in the central region of the star during its evolution toward the white dwarf stage. Therefore, a core of carbon-burning products and an envelope of C^{12} were assumed for our model. The major properties of the model constructed in this manner are summarized in Table III.

TABLE III

Properties of the white dwarf model

Mass $= 1.373\ M_\odot$
Central density $= 10^{9.5}$ gm/cm^3
Radius = 1810 km
Radius of URCA shell = 377 km
URCA nuclear pair Na^{23} and Ne^{23}
Core of $1M_\odot$ of carbon-burning products
Envelope of C^{12}
Period = 2.26 sec

Composition of core

Mass number	Mass fraction	Nuclei and electron capture thresholds (MeV)
16	0.01	O^{16} (10.4) C^{16}
20	0.41	Ne^{20} (7.03) O^{20} (21.22) C^{20}
23	0.06	Na^{23} (4.4) Ne^{23} (11.15) F^{23} (13.87) O^{23}
24	0.52	Mg^{24} (5.52) Ne^{24} (15.91) O^{24}

The composition of the core was based on the results obtained by Arnett and Truran (1969) for carbon burning near 10^9 K. The charge number of these nuclei depends on the density. The carbon-burning products that are normally stable are on the left-hand side in the table, but as the density increases, as soon as the threshold energy (which is shown in MeV in the table) is exceeded by the electron Fermi energy, these nuclei capture electrons changing into more neutron-rich isobars (toward the right in Table III). We used a core mass of $M_\odot/2$ in our later calculations, but this produced no significant change in our final results.

The flux from an URCA shell of the $Na^{23}-Ne^{23}$ pair has been calculated by use of Equation (12). The following value of a_0 was used, which was obtained for this particular model of a white dwarf:

$$a_0 = 9.50 \times 10^{-8}\ \text{cm}^{-1}, \quad |\mathrm{d}E_F/\mathrm{d}r| = a_0 m_e c^2 = 4.854 \times 10^{-8}\ \text{MeV/cm}.$$

The flux obtained in this manner has to be multiplied by the factor χ defined by (27) in order to take the composition into account. In our present case,

$$\chi \approx \chi_{Na^{23}} = 0.06.$$

The total neutrino energy loss rate from the URCA shell (and hence from the star) is given by

$$\mathscr{L} = 4\pi r_s^2 \chi F , \tag{29}$$

where r_s is the radius of the URCA shell, and F is obtained from Equation (12).

The cooling time of the star is then obtained by

$$\tau = \int_{E(0)}^{E(\tau)} \frac{\mathrm{d}E}{\mathscr{L}(E)} ; \tag{30}$$

$E(0)$ is the initial total energy of the star at $t=0$, and $E(\tau)$ is the total energy at $t=\tau$. The total energy of the star is given by

$$E = E_{th} + E_v , \tag{31}$$

where E_{th} is the thermal energy and E_v is the vibrational energy expressed as

$$\begin{aligned} E_{th} &= \int_0^R Un4\pi r^2 \, \mathrm{d}r = a_{th} T \\ E_v &= \int_0^R \tfrac{1}{2}\varrho v^2 4\pi r^2 \, \mathrm{d}r = a_v \xi_0^2 , \end{aligned} \tag{32}$$

where

$$\begin{aligned} a_{th} &= C_v N_0 \left(\sum_j \frac{\chi_j}{A_j} \right) \int_0^R \varrho 4\pi r^2 \, \mathrm{d}r \\ &= C_v N_0 M \left(\frac{\bar{1}}{A} \right), \quad \left(\frac{\bar{1}}{A} \right) \equiv \sum_{j=1}^{m} \frac{\chi_j}{A_j} , \end{aligned} \tag{33}$$

and

$$a_v = \frac{(2\pi)^3}{P_v^2} \int_0^R \varrho r^4 \, \mathrm{d}r .$$

In the above expressions, $U = C_v T$ is the thermal energy per ion, C_v is the specific heat, n is the total number density of the ions (including all nuclear species), v is the velocity due to radial oscillation, N_0 is Avogadro's number, M is the total mass of the star, and P_v is the period of vibration. We used $P_v = 2.26$ sec, which was taken from the corresponding white dwarf model in Cohen *et al.* (1969). The core integration of the quantity $\varrho\, r^4$ has been carried out to obtain a_v in (33).

If the ions are in the state of an ideal gas, the specific heat $C_v = (\frac{3}{2})k$. However, it is possible that as the star cools down, the matter becomes crystallized at a certain critical temperature T_c (Van Horn, 1968). Therefore, we considered both cases. The specific heat in crystals can be expressed as

$$C_v \cong 3k\mathscr{D}(\theta/T),$$

where $\mathscr{D}(\theta/T)$ is the Debye function. It approaches 1 for $T \gg \theta$, and varies as $(T/\theta)^3$ for $T \ll \theta$ (θ is the Debye temperature). The numerical values of $\mathscr{D}$ in the intermediate regions are given by Landau and Lifshitz (1958, p. 189). It is unrealistic to assume that suddenly a perfect gas will change to crystals at T_c. Rather, it is more likely that there are certain regions above T_c where a gradual phase change will take place through a liquid-like intermediate phase, where C_v/k will change gradually from $\frac{3}{2}$ to 3 as the temperature decreases toward T_c. These and other features have been discussed in Brush *et al.* (1966) and Van Horn (1968), and we used their work to estimate the critical temperature T_c (where the crystallization takes place), the behavior in the liquid-like region, and other quantities, such as the heat released and added to the thermal energy at the point of crystallization.

From the expressions for $\mathscr{L}$ and F, we see that the total energy loss rate $\mathscr{L}$ can be separated into the thermal component $\mathscr{L}_{th}(T)$ and the vibrational component $\mathscr{L}_v(\xi_0)$, as was done for the total energy E (Equation (31)). Therefore, we assumed that the thermal and the vibrational components are decoupled in Equation (30) also, with τ_{th} expressing cooling time and τ_v expressing vibrational damping time. A more accurate treatment would include some heating effects due to vibrational damping. The results are shown in Figure 9. The solid straight line shows the cooling of stars with $C_v = (\frac{3}{2})k$, which applies to an ideal gas. Here, internal temperature T is plotted against time. The results shown in Figure 9 are independent of the exact value of the initial temperature used, provided it is sufficiently high. The other solid curve in Figure 9 is the cooling curve with the crystallization included. We note the deviation from the ideal gas case starting at around 2×10^8 K, with slightly higher temperatures at any given time. This is due to the gradual increase in specific heat C_v, from the ideal gas value of $(\frac{3}{2})k$ to $3k$, as the temperature decreases and the phase change takes place

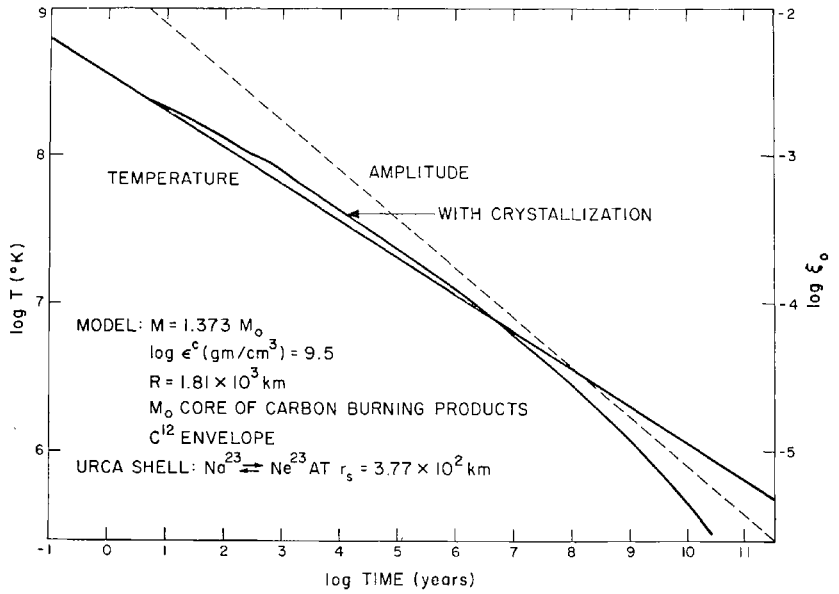

Fig. 9. Cooling and vibrational damping of a white dwarf model whose properties are as shown.

through the intermediate liquid-like phase. In our model, the crystallization takes place at around 10^8 K, with a small hump at that point in Figure 9 indicating the effect of the released latent heat. With a further decrease in temperature, the cooling rate of the crystal increases compared to the case of an ideal gas, owing to the decrease of specific heat caused by the Debye factor. On a time scale of 10^9 yr, which is a typical age of white dwarfs, the internal temperature is seen to be about two million degrees without crystallization and about a million degrees with crystallization. It should be noted that additional cooling by surface electromagnetic radiation has been completely neglected in these illustrative calculations. The dashed line in Figure 9 shows vibrational damping with time. Here again, the results shown are insensitive to the exact value used for the initial amplitude. After 10^9 yr, the vibrational amplitude is reduced to about 2×10^{-5}.

The above results are consistent with observations by Greenstein (1968), who has found that there is a real absence of faint blue white dwarfs, an absence that is not due simply to selection effects or inadequate statistics. We note that there are still uncertainties connected with the problem of crystallization of white dwarfs. For instance, some authors may consider that the crystallization is not a first-order phase change and thus that the heat would not be released at T_c (Mestel and Ruderman, 1967). However, such uncertainty can affect our results only around 10^8 K, and even there it can do so only slightly. Our results obtained at temperatures below $\sim 10^7$ K, and hence for time scales longer than 10^6 yr, are unaffected by such uncertainties, and the above conclusion about the observational aspects of faint blue white dwarfs is still valid.

6. Comparison with Other Neutrino Processes

Among other neutrino reactions that are of interest in stellar problems, the following three are found to be of particular importance: the plasma neutrino process, the pair neutrino process, and the photoneutrino process. Beaudet *et al.* (1967) reviewed these problems and gave a convenient analytic formula for the combination of the three reactions that is accurate to within 15%. Hansen (1968) gave a simpler, but less accurate expression (a maximum error of 30%). Other, earlier references are found in the above two papers.

In order to estimate the contribution from 'other reactions', we used the first reference (Beaudet *et al.*, 1967) because of the greater accuracy and convenience. It is not easy to compare exactly the importance of the URCA process with that of other neutrino processes without further information on the stellar model in question, because the contribution from the URCA process is only from a narrow range of density (near $W_m = W_F$), and thus it is not practical to talk about energy rate per unit volume Q (or per unit mass), in which other neutrino rates are generally expressed. In order to make a more realistic comparison, we have to compare $\mathscr{L}$, the total energy loss per unit time from the star (in ergs/sec). For this purpose, an actual stellar model has to be constructed, and we used the white dwarf model of Section 5. The total URCA energy per unit time, $\mathscr{L}^U$, was obtained through Equation (29), and the energy rates

due to other processes, $\mathscr{L}^0$, were calculated through the integration

$$\mathscr{L}^0 = \int_0^R Q_{\text{tot}} 4\pi r^2 \, dr,$$

where Q_{tot} was obtained through the analytic expression given by Beaudet *et al.* (1967). The results are shown in Figure 10 (the solid curve), where the ratio $\mathscr{L}^U/\mathscr{L}^0$ is plotted against temperature. We note that for temperatures up to about 2×10^9 K, the URCA neutrinos give the greatest contribution. We also considered an URCA shell of the

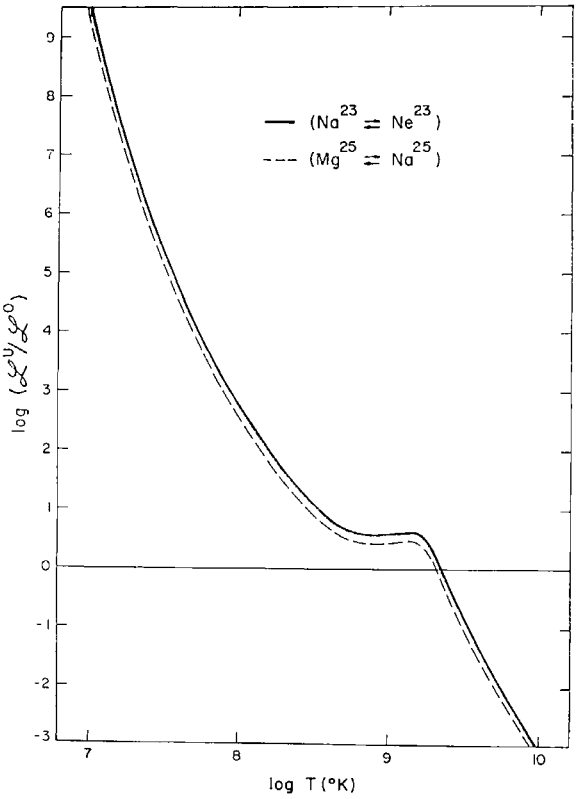

Fig. 10. The comparison between the URCA process and other neutrino processes: $\mathscr{L}^U$ is the URCA energy loss per unit time from the star (ergs/sec) and $\mathscr{L}^0$ is the total energy loss per unit time from the star due to other neutrino processes. A white dwarf model of Figure 9 was used for the case of the $Na^{23} - Ne^{23}$ pair. A similar white dwarf model was used for the pair $Mg^{25} - Na^{25}$.

$Mg^{25} - Na^{25}$ pair in a similar model, assuming that the mass fraction of the URCA pair is again 0.06%. The result is shown by the dashed curve in Figure 10. We conclude that in the critical regions of 10^7 K to 2×10^9 K, the URCA process dominates over other possible neutrino reactions, and thus the URCA energy loss seems far more important than estimated earlier.

Appendix 1

The basic Equations (2)–(3) of Section 2 can be expressed as (Hansen, 1966)

$$\begin{aligned}
\lambda^+ &= C^+ I_1^+ , \\
L^+ &= C^+ (I_2^+ - W_m I_1^+), \\
\lambda^- &= C^- (I_1^- - I_2^-), \\
L^- &= C^- [W_m (I_1^- - I_2^-) - (I_3^- - I_4^-)],
\end{aligned} \tag{A1}$$

where for relativistic electrons ($W \approx P$),

$$\begin{aligned}
I_1^+ &= \int_{W_m}^{\infty} W^2 (W_m - W)^2 S \, \mathrm{d}W , \\
I_2^+ &= \int_{W_m}^{\infty} W^3 (W_m - W)^2 S \, \mathrm{d}W , \\
I_1^- &= \int_{1}^{W_m} W^2 (W_m - W)^2 \, \mathrm{d}W = E(-W_m, W_m), \\
I_2^- &= \int_{1}^{W_m} W^2 (W_m - W)^2 S \, \mathrm{d}W , \\
I_3^- &= \int_{1}^{W_m} W^3 (W_m - W)^2 \, \mathrm{d}W = H(-W_m, W_m), \\
I_4^- &= \int_{1}^{W_m} W^3 (W_m - W)^2 S \, \mathrm{d}W ;
\end{aligned} \tag{A2}$$

$$\begin{aligned}
E(x, y) &= x^2 \left(\frac{y^3 - 1}{3} \right) + x \left(\frac{y^4 - 1}{2} \right) + \left(\frac{y^5 - 1}{5} \right), \\
H(x, y) &= x^2 \left(\frac{y^4 - 1}{4} \right) + 2x \left(\frac{y^5 - 1}{5} \right) + \left(\frac{y^6 - 1}{6} \right).
\end{aligned} \tag{A3}$$

The Coulomb factor $F^{\pm}(Z, W)$ in (2) takes the form (25). In our present analytic investigation, we can replace W/P in Equation (25) by W_m/P_m (the energy per momentum at the threshold point) and take it out of the integral. Then $C^{\pm}$ above can be expressed as Equation (16).

After expanding

$$S = \{1 + \exp[\beta(W - W_F)]\}^{-1} \tag{A4}$$

and integrating, we can summarize the results as follows:

$$I_1^+ = W_m^5 E(-1, u') + I_{12}^+ \quad \text{for} \quad W_F \geqslant W_m,$$

where

$$I_{12}^+ = W_m^5 \sum_{l=1}^{5} \frac{1}{\beta'^l} [\eta(l, t'^{-1}) D_l(1, -1) - \eta(l, 1) D_l(u', -1) + \eta(l, 1) D_l(-u', 1)]; \tag{A5}$$

and

$$I_1^+ = W_m^5 \sum_{l=1}^{5} \frac{1}{\beta'^l} \eta(l, t') D_l(-1, 1) \quad \text{for} \quad W_F \leqslant W_m;$$

$$I_2^+ = W_m^6 H(-1, u') + I_{22}^+ \quad \text{for} \quad W_F \geqslant W_m,$$

where

$$I_{22}^+ = W_m^6 \sum_{l=1}^{6} \frac{1}{\beta'^l} [\eta(l, t'^{-1}) G_l(1, -1) - \eta(l, 1) G_l(u', -1) - \eta(l, 1) G_l(-u', 1)]; \tag{A6}$$

and

$$I_2^+ = W_m^6 \sum_{l=1}^{6} \left[-\frac{1}{\beta'^l} \eta(l, t') G_l(-1, 1) \right] \quad \text{if} \quad W_F \leqslant W_m.$$

In Equations (A5) and (A6),

$$\begin{aligned} t' &= \exp[\beta'(u' - 1)] = \exp \beta(W_F - W_m), \\ \beta' &= \beta W_m, \quad u' = W_F/W_m, \end{aligned} \tag{A7}$$

and

$$\eta(l, t) = \sum_{n=1}^{\infty} \frac{t^n}{n^l} (-1)^{n+1} = t - \frac{t^2}{2^l} + \cdots, \quad \text{for} \quad t < 1. \tag{A8}$$

In (A5),

$$\begin{aligned} D_1(x, y) &= x^2(y + x)^2, \\ D_2(x, y) &= -2x(x + y)(2x + y), \\ D_3(x, y) &= 2(6x^2 + 6xy + y^2), \\ D_4(x, y) &= -12(2x + y), \\ D_5(x, y) &= 24; \end{aligned} \tag{A9}$$

and in (A6),

$$\begin{aligned} G_1(x, y) &= x^3(x + y)^2, \\ G_2(x, y) &= -x^2(x + y)(5x + 3y), \\ G_3(x, y) &= 2x(10x^2 + 12xy + 3y^2), \\ G_4(x, y) &= -6(10x^2 + 8xy + y^2), \\ G_5(x, y) &= 24(5x + 2y), \\ G_6(x, y) &= -120. \end{aligned} \tag{A10}$$

Similarly,

$$I_2^- = E(-W_m, W_m) + I_{21}^- \quad \text{for} \quad W_F \geq W_m,$$

where

$$I_{21}^- = \sum_{l=1}^{5} \frac{1}{\beta^l} [\eta(l, t^{-1}) D_l(1, -W_m) - \eta(l, t_m^{-1}) D_l(W_m, -W_m)]; \tag{A11a}$$

and

$$I_2^- = E(-W_m, W_F) + I_{22}^- \quad \text{for} \quad W_F \leq W_m,$$

where

$$I_{22}^- = \sum_{l=1}^{5} \frac{1}{\beta^l} [\eta(l, t^{-1}) D_l(1, -W_m) - \eta(l, 1) D_l(W_F, -W_m) + \eta(l, 1) D_l(-W_F, W_m) - \eta(l, t_m) D_l(-W_m, W_m)]; \tag{A11b}$$

$$I_4^- = H(-W_m, W_m) + I_{41}^- \quad \text{for} \quad W_F \geq W_m,$$

where

$$I_{41}^- = \sum_{l=1}^{6} \frac{1}{\beta^l} [\eta(l, t^{-1}) G_l(1, -W_m) - \eta(l, t_m^{-1}) G_l(W_m, -W_m)]; \tag{A12a}$$

and

$$I_4^- = H(-W_m, W_F) + I_{42}^- \quad \text{for} \quad W_F \leq W_m,$$

where

$$I_{42}^- = \sum_{l=1}^{6} \frac{1}{\beta^l} [\eta(l, t^{-1}) G_l(1, -W_m) - \eta(l, 1) G_l(W_F, -W_m) - \eta(l, 1) G_l(-W_F, W_m) + \eta(l, t_m) G_l(-W_m, W_m)]. \tag{A12b}$$

In Equations (A11a)–(A12b),

$$t = \exp[\beta(W_F - 1)]; \quad t_m = \exp[\beta(W_F - W_m)]. \tag{A13}$$

From Equations (A2) and (A3),

$$I_1^- = E(-W_m, W_m) = \frac{W_m^5}{30} - \frac{W_m^2}{3} + \frac{W_m}{2} - \frac{1}{5}$$

and

$$I_3^- = H(-W_m, W_m) = \frac{W_m^6}{60} - \frac{W_m^2}{4} + \frac{2}{5} W_m - \frac{1}{6}. \tag{A14}$$

Also,

$$E(-1, u') = \frac{u'^3}{3} - \frac{u'^4}{2} + \frac{u'^5}{5} - \frac{1}{30} = \frac{\Delta^3}{3} + \frac{\Delta^4}{2} + (\text{higher order terms in powers of } \Delta), \tag{A15}$$

$$H(-1, u') = \frac{\Delta^3}{3} + \frac{3}{4}\Delta^4 + (\text{higher order terms in powers of } \Delta),$$

where we defined the width Δ as

$$\Delta \equiv |W_F - W_m|/W_m = |u' - 1| . \tag{A16}$$

Similarly,

$$\begin{aligned} E(-W_m, W_m) - E(-W_m, W_F) &= W_m^5\left(-\frac{\Delta^3}{3} - \frac{\Delta^4}{2}\right) \\ &\quad + (\text{higher order terms in powers of } \Delta), \\ H(-W_m, W_m) - H(-W_m, W_F) &= W_m^6\left(-\frac{\Delta^3}{3} - \frac{3}{4}\Delta^4\right) \\ &\quad + (\text{higher order terms in powers of } \Delta). \end{aligned} \tag{A17}$$

From (A5)–(A10) and (A15), we obtain for $W_F \geqslant W_m$,

$$\begin{aligned} I_1^+ &= W_m^5\left\{\frac{\Delta^3}{3} + \frac{\Delta^4}{2} + \eta(2,1)\,\beta'^{-2}4u'(u'-1)(2u'-1)\right. \\ &\quad \left. + \beta'^{-3}2\eta(3,t'^{-1}) + \beta'^{-4}[24(2u'-1)\eta(4,1) - 12\eta(4,t'^{-1})]\right\} \\ I_2^+ &= W_m^6\left\{\frac{\Delta^3}{3} + \frac{3}{4}\Delta^4 + \eta(2,1)\,\beta'^{-2}2u'^2\right. \\ &\quad \times (5u'-3)(u'-1) + \beta'^{-3}2\eta(3,t'^{-1}) \\ &\quad \left. + \beta'^{-4}[12(10u'^2 - 8u' + 1)\eta(4,1) - 18\eta(4,t'^{-1})]\right\}; \end{aligned} \tag{A18}$$

and for $W_F \leqslant W_m$,

$$\begin{aligned} I_1^+ &= W_m^5[\beta'^{-3}2\eta(3,t') + \beta'^{-4}12\eta(4,t')], \\ I_2^+ &= W_m^6[\beta'^{-3}2\eta(3,t') + \beta'^{-4}18\eta(4,t')]. \end{aligned}$$

For semidegenerate electrons, t in $\eta(l,t)$ (Equation (A8)) is always very small, and thus we can retain only the first term of the expansion in (A8). Then,

$$\eta(l,t) = t . \tag{A19}$$

Applying this to Equation (A18), together with (A1) and (A7), we finally obtain: for $W_F \geqslant W_m$,

$$\begin{aligned} \lambda^+ &= C^+ W_m^5\left[\frac{\Delta^3}{3} + \frac{1}{\beta'^2}f_1(\Delta) + \frac{2}{\beta'^3}\exp(-\beta'\Delta)\right] \\ L^+ &= C^+ W_m^6\left\{\frac{\Delta^4}{4} + \frac{1}{\beta'^2}f_2(\Delta) + \frac{1}{\beta'^4}[f_3(\Delta) - 6\exp(-\beta'\Delta)]\right\}; \end{aligned} \tag{A20a}$$

and for $W_F \leqslant W_m$,

$$\begin{aligned} \lambda^+ &= C^+ W_m^5 \frac{2}{\beta'^3}\exp(-\beta'\Delta), \\ L^+ &= C^+ W_m^6 \frac{6}{\beta'^4}\exp(-\beta'\Delta), \end{aligned} \tag{A20b}$$

$$f_1(\Delta) = 4u'(2u' - 1)\,\Delta = 4(2\Delta - 1)(\Delta + 1)\,\Delta,$$
$$f_2(\Delta) = 2u'(5u'^2 - 7u' + 2)\,\Delta = 2(5\Delta + 3)(\Delta + 1)\,\Delta^2, \tag{A21}$$
$$f_3(\Delta) = 12(10u'^2 - 12u' + 3) = 12(10\Delta^2 + 8\Delta + 1).$$

In the above derivation, we used relation (A16) for Δ. Also, we neglected the higher order terms of Δ, β'^{-1} and the mixed term because they are small (note that in our present consideration, $W_F \approx W_m$ and $kT \ll E_F$).

We obtained β^- decay rates in a similar manner. The results follow: for $W_F \geqslant W_m$,

$$\lambda^- = C^- W_m^5 \left(\frac{2}{\beta'^3}\right) \exp(-\beta'\Delta),$$
$$L^- = C^- W_m^6 \left(\frac{6}{\beta'^4}\right) \exp(-\beta'\Delta); \tag{A22a}$$

for $W_F \leqslant W_m$,

$$\lambda^- = C^- W_m^5 \left[\frac{\Delta^3}{3} + \frac{1}{\beta'^2} f_1(\Delta) + \frac{2}{\beta'^3} \exp(-\beta'\Delta)\right],$$
$$L^- = C^- W_m^6 \left\{\frac{\Delta^4}{4} + \frac{1}{\beta'^2} f_2(\Delta) + \frac{1}{\beta'^4} [f_3(\Delta) - 6\exp(-\beta'\Delta)]\right\}, \tag{A22b}$$

where $f_i(\Delta)$'s are as defined in (A21). In the above derivation, the relations (A1), (A7) through (A14), (A16), (A17), and (A19) are used.

Appendix 2

From (13) of Section 3,

$$\Delta = |W_F - W_m|/W_m. \tag{A23}$$

Denoting the equilibrium values by the subscript 0 as before, we have

$$\Delta_0 = |W_{F0} - W_m|/W_m. \tag{A24}$$

Then, using Equations (7) and (8), we have

$$\Delta = |W_{F0} + dW_F - W_m|/W_m = \Delta_0 + \delta, \tag{A25}$$

where δ is defined as

$$\delta = dW_F/W_m = -u'_0 \xi_0 \sin\omega t, \quad u'_0 = W_{F0}/W_m. \tag{A26}$$

In (A26), ξ_0 is the amplitude at the maximum point of expansion and compression. Substituting (A25) in Equation (18), we obtain

$$\lambda = a_\lambda(\Delta_0 + \delta)^3 + b_\lambda T^3 = \lambda_\Delta + \lambda_{th},$$
$$L = a_L(\Delta_0 + \delta)^4 + b_L T^4 = L_\Delta + L_{th}. \tag{A27}$$

Here, we dropped the superscripts $(\pm)$ for convenience, because we get similar expressions for electron captures and beta decays.

Since δ involves time, we have to integrate expressions (A27) over a period to obtain the total rates. Then,

$$\begin{aligned}\lambda_\Delta &\equiv \lambda(T=0)\\ &= a_\lambda(\Delta_0^3 + 3\Delta_0^2 u_0' \xi_0 I_{t1} + 3\Delta_0 u_0'^2 \xi_0^2 I_{t2} + u_0'^3 \xi_0^3 I_{t3}),\end{aligned}$$

and

$$\begin{aligned}L_\Delta &\equiv L(T=0)\\ &= a_L(\Delta_0^4 + 4\Delta_0^3 u_0' \xi_0 I_{t1} + 6\Delta_0^2 u_0'^2 \xi_0^2 I_{t2} + 4\Delta_0 u_0'^3 \xi_0^3 I_{t3}\\ &\quad + u_0'^4 \xi_0^4 I_{t4}).\end{aligned} \tag{A28}$$

The integrals I_{ti}'s in (A28) are defined as

$$I_{ti} = \left[\int_0^{2\pi/\omega} (-\sin\omega t)^i \, dt \Big/ \int_0^{2\pi/\omega} dt\right] = \frac{1}{\pi}\int_0^{\pi/2} \sin^i\theta \, d\theta,$$

and we obtain (A29)

$$I_{t1} = \frac{1}{\pi}, \quad I_{t2} = \frac{1}{4}, \quad I_{t3} = \frac{2}{3\pi}, \quad I_{t4} = \frac{3}{16}.$$

Using (A29), we can summarize the expressions in (A28) as

$$\lambda_\Delta = a_\lambda \sum_{n=0}^{3} a_n' \Delta_0^{3-n} u_0'^n \xi_0^n$$

and (A30)

$$L_\Delta = a_L \sum_{n=0}^{4} b_n' \Delta_0^{4-n} u_0'^n \xi_0^n,$$

where

$$a_0' = 1, \quad a_1' = \frac{3}{\pi}, \quad a_2' = \frac{3}{4}, \quad a_3' = \frac{2}{3\pi}$$

and (A31)

$$b_0' = 1, \quad b_1' = \frac{4}{\pi}, \quad b_2' = \frac{3}{2}, \quad b_3' = \frac{8}{3\pi}, \quad b_4' = \frac{3}{16}.$$

Substituting (A30) into Equation (A27), we get Equation (22) in Section 3.

When $\Delta_0 = 0$, using (A30) and (A31) we obtain

$$\lambda_\Delta = a_\lambda\left(\frac{2}{3\pi}\right) u_0'^3 \xi_0^3 \quad \text{and} \quad L_\Delta = a_L\left(\frac{3}{16}\right) u_0'^4 \xi_0^4.$$

Appendix 3

Here, we confine ourselves to the case $W_m \gg 1$, for the analytic solution of Equation (12) is otherwise hopeless. Also, since the contribution to F comes only in the region

near $W_F = W_m$, we have $W_F \gg 1$. Thus, we can write (12) as

$$F^{\pm} = \left(\frac{a_\mu}{Z}\frac{1}{a_0}\right)\int_{W_{F1}}^{W_{F2}} W_{F0}^3 \left(\frac{L^{\pm}\lambda^{\mp}}{\lambda^+ + \lambda^-}\right) dW_{F0}\,, \tag{A32}$$

where we used the approximation

$$W_F^3 = W_{F0}^3(1 - \xi_0 \sin\omega t)^3 \simeq W_{F0}^3\,,$$

because $\xi_0 < 1$ always and $\sin\omega t \leqslant 1$ always (in the range of our interest, we have $\xi_0 \leqslant 0.1$).

Owing to the symmetry in the expressions of $L^{\pm}$ and $\lambda^{\pm}$ about the point $W_m = W_{F0}$ (see Equations (14) and (15)), (A32) can be expressed as

$$F^{\pm} = 2\left(\frac{a_\mu}{Z}\frac{1}{a_0}\right)\int_0^{\Delta_1} W_{F0}^3 \left(\frac{L^{\pm}\lambda^{\mp}}{\lambda^+ + \lambda^-}\right) W_m\, d\Delta_0\,, \tag{A32'}$$

where Δ_0 is defined by (A24), and Δ_1 is the half width of the URCA shell in units of W_m.

In the region near $W_{F0} = W_m$, we get from Equations (19) and (23)

$$\left(\frac{L^{\pm}\lambda^{\mp}}{\lambda^+ + \lambda^-}\right) = \left(\tfrac{3}{16}a_L^{\pm}u_0'^4\xi_0^4 + b_L^{\pm}T^4\right)\left(\frac{C^{\mp}}{C^+ + C^-}\right). \tag{A33}$$

From (A32') and (A33),

$$F^{\pm} = C_F^{\pm}\left[\int_0^{\Delta_1} u_0'^3\left(\tfrac{3}{16}a_L^{\pm}u_0'^4\xi_0^4 + b_L^{\pm}T^4\right) d\Delta_0\right] = F_v^{\pm} + F_{th}^{\pm}\,,$$

where (A34)

$$C_F^{\pm} = \left(\frac{2a_\mu}{a_0 Z}\right)\left(\frac{C^{\mp}}{C^+ + C^-}\right) W_m^4\,;$$

u_0' is defined by (A26),

$$F_v^{\pm} = C_F^{\pm}\,\tfrac{3}{16}a_L^{\pm}\xi_0^4\int_0^{\Delta_1} u_0'^7\, d\Delta_0$$

is the vibrational component, and

$$F_{th}^{\pm} = C_F^{\pm}b_L^{\pm}T^4\int_0^{\Delta_1} u_0'^3\, d\Delta_0$$

is the thermal component. Noting that $\Delta_1 \sim \delta_{max} = u_0'\xi/2$ for vibration, $\Delta_1 \sim 1/\beta'$

without vibration, and that $\Delta_1 \ll 1$, we obtain

$$F_v^{\pm} = C_F^{\pm} \frac{3}{32\pi} a_L^{\pm} \xi_0^5$$

and (A35)

$$F_{th}^{\pm} = C_F^{\pm} b_L^{\pm} T^4 \frac{1}{\beta'} = C_F^{\pm} b_L^{\pm} \frac{1}{W_m} \frac{k}{m_e c^2} T^5,$$

using the relation (13) for β'.

Substituting (16) into the second equation of (A34), we get

$$C_F^{\pm} = \left(\frac{2a_\mu}{a_0 Z}\right) \frac{\langle F\rangle^{\mp}}{\langle F\rangle^{+} + \langle F\rangle^{-}} W_m^4. \tag{A36}$$

From (16), (19), (A34), (A35), and (A36), we obtain

$$F^{\pm} = \left(\frac{\ln 2}{ft}\right)\left(\frac{a_\mu}{a_0 Z}\right)\left(\frac{\langle F\rangle^{\pm}\langle F\rangle^{\mp}}{\langle F\rangle^{+} + \langle F\rangle^{-}}\right) 3 W_m^{10} \left(\frac{1}{64\pi} \xi_0^5 + 4 \frac{1}{\beta'^5}\right). \tag{A37}$$

The total flux of Equation (24) is then obtained from the sum of F^+ and F^- above with the use of the definition of β' in (13).

Appendix 4

Let us consider the electron capture rate

$$\lambda^+ = C^+ \int_{W_m}^{\infty} WP(W - W_m)^2 S \, dW,$$

$$C^+ = \frac{\ln 2}{ft} \langle F\rangle^+, \tag{A38}$$

$$S = \{1 + \exp[\beta(W - W_F)]\}^{-1}, \quad P = \sqrt{W^2 - 1}.$$

For $W_F \geqslant W_m$,

$$\lambda^+ = C^+ \left(\int_{W_m}^{W_F} d\lambda^+ + \int_{W_F}^{\infty} d\lambda^+\right),$$

where

$$d\lambda^+ = WP(W - W_m)^2 S \, dW.$$

Expanding S, we get

$$\lambda^{+\prime} \equiv \frac{\lambda^+}{C^+} = \int_{W_m}^{W_F} WP(W - W_m)^2 \, dW$$
$$+ \sum_{n=1}^{\infty} (-1)^n \int_{W_m}^{W_F} WP(W - W_m)^2 \exp[-n\beta(W_F - W)] \, dW$$
$$+ \sum_{n=1}^{\infty} (-1)^{n+1} \int_{W_F}^{\infty} WP(W - W_m)^2 \exp[-n\beta(W - W_F)] \, dW. \tag{A39}$$

After the above integrations are carried out, the result can be expressed as

$$\lambda^{+\prime} = \lambda_{\Delta}^{+\prime} + \lambda_{\mathrm{T}}^{+\prime}. \tag{A40}$$

From the first term of (A39), we get

$$\lambda_{\Delta}^{+\prime} = \lambda_{\Delta}^{+\prime}(W_{\mathrm{F}}, P_{\mathrm{F}}) - \lambda_{\Delta}^{+\prime}(W_m, P_m),$$

where

$$\lambda_{\Delta}^{+\prime}(y, x) = \frac{x^5}{5} + \frac{x^3}{3}(W_m^2 + 1) - W_m\left[\tfrac{1}{2}xy^3 - \tfrac{1}{4}xy - \tfrac{1}{4}\ln(x + y)\right]. \tag{A41}$$

For vibration, we use the relations (7) and (8). Then, at $W_{\mathrm{F}0} = W_m$, after lengthy calculations, Equations (A41) reduce approximately to

$$\lambda_{\Delta}^{+\prime}(W_{\mathrm{F}0} = W_m) \equiv \lambda_{\xi}^{+\prime} = a_{\xi 3}(W_m)\, I_{t3}\xi_0^3 + (\text{higher order terms of } \xi_0), \tag{A42}$$

where I_{t3} is the time integral defined in (A29), and $a_{\xi 3}$ is a function of W_m expressed as

$$a_{\xi 3} = \frac{1}{3}P_m^5 + \frac{7}{6}P_m^3\left(1 - \frac{5}{14}\frac{1}{W_m^2}\right)$$
$$P_m = \sqrt{W_m^2 - 1}. \tag{A43}$$

Similarly, from the integration of the last two terms of (A39), we obtain at $W_{\mathrm{F}0} = W_m$ roughly

$$\lambda_{\mathrm{T}}^{+\prime} = 3a_{\xi 3}(W_m)\left[\frac{1}{\beta'^2}\, 4u_0'(2u_0' - 1)\, I_{t1}\xi_0 + \frac{2}{\beta'^3}\right] + (\text{higher order terms of } T), \tag{A44}$$

where β' and u_0' are as defined earlier in (13) and (A26). Thus, from (A40), (A42), and (A44) for $W_{\mathrm{F}0} = W_m$ we obtain

$$\lambda^+ = C^+\lambda^{+\prime} = C^+\left[a_{\xi 3}I_{t3}\xi_0^3 + \frac{6a_{\xi 3}}{\beta'^3} + \frac{3a_{\xi 3}}{\beta'^2}\, 4u_0'(2u_0' - 1)\, I_{t1}\xi_0\right]. \tag{A45}$$

We would have obtained the same expression if we had started with the region $W_{\mathrm{F}} \leqslant W_m$. In (A45), only the lowest terms in ξ_0, β'^{-1} and the mixed term have been retained. Even so, we note that the rate λ^+ is a complicated function of W_m.

From the expressions for $a_{\xi 3}$ given in (A43), we may find some physical insight in the above result. For large W_m, $a_{\xi 3} \to W_m^5/3$. Thus, we get

$$\lambda_{\xi}^+ \to C^+\left(\frac{W_m^5}{3}\right) I_{t3}\xi_0^3 \tag{A46}$$

as expected.

Similar results are also obtained for the beta decay rate λ^-. Some of the integrals involved in the expressions $L^{\pm}$ cannot be solved analytically, and thus we cannot extend our present work to these cases. However, we expect similar results for them also (see Section 4).

Appendix 5

Let us suppose we have m nuclear species and denote the number density of the nucleus j as n_j and the mass fraction of j as χ_j. Then,

$$\varrho = \sum_{j=1}^{m} A_j n_j / N_0 , \quad \varrho_i = A_i n_i / N_0 , \tag{A47}$$

$$\chi_i \equiv \varrho_i / \varrho . \tag{A48}$$

Thus,

$$n_i = \chi_i \varrho N_0 / A_i . \tag{A49}$$

Now, from charge neutrality, using (A49) we get

$$n_e = \sum_{j=1}^{m} Z_j n_j = \left(\sum_{j=1}^{m} \chi_j \frac{Z_j}{A_j} \right) \varrho N_0 = \frac{\varrho N_0}{\bar{\mu}_e} , \tag{A50}$$

where

$$\bar{\mu}_e = \left(\sum_{j=1}^{m} \chi_j \frac{Z_j}{A_j} \right)^{-1} \equiv \left\langle \frac{\bar{A}}{Z} \right\rangle . \tag{A51}$$

Also, $n_e = a_\mu (W_F^2 - 1)^{3/2}$ from (6). Then, from (A49), (A50), and (6), we obtain

$$n_i = \left(\frac{\chi_i}{A_i} \right) \bar{\mu}_e a_\mu (W_F^2 - 1)^{3/2} .$$

Or, with slight rearrangement, it can be expressed as

$$n_i = \chi \frac{a_\mu}{Z_i} (W_F^2 - 1)^{3/2} ,$$

where χ is defined as $\chi = \chi_i \bar{\mu}_e / \mu_e$, with $\mu_e = A_i / Z_i$ and $\bar{\mu}_e$ given by (A51). Now let us consider that $n_i = n_i^+ + n_i^-$ is the number density of a pair of URCA nuclei. From the steady-state condition, $\lambda^+ n_i^+ = \lambda^- n_i^-$. From these relations, we get

$$n_i^{\pm} = \frac{\lambda^{\mp}}{\lambda^+ + \lambda^-} n_i = \chi \left[\frac{a_\mu}{Z_i} (W_F^2 - 1)^{3/2} \left(\frac{\lambda^{\mp}}{\lambda^+ + \lambda^-} \right) \right] . \tag{A52}$$

Comparing (A52) with Equation (11) of Section 2, we see that, for a composite matter, the number density of the URCA nuclei $n^{\pm}$ appearing in (9) must be multiplied by χ, and thus the flux for a composite matter is χ times the flux without other species, which is given by (12).

Acknowledgements

This work was supported in part by the U.S. Atomic Energy Commission, the National Science Foundation, and the National Aeronautics and Space Administration.

References

Arnett, W. D.: 1969, *Astrophys. Space Sci.* **5**, 180.
Arnett, W. D. and Truran, J. W.: 1969, private communication.
Bahcall, J. N.: 1962, *Phys. Rev.* **126**, 1143.
Bahcall, J. N.: 1964, *Astrophys. J.* **139**, 318.
Beaudet, G., Petrosian, V., and Salpeter, E. E.: 1967, *Astrophys. J.* **150**, 979.
Brush, S. G., Sahlin, H. L., and Teller, E.: 1966, *J. Chem. Phys.* **45**, 2102.
Cohen, J. M., Lapidus, A., and Cameron, A. G. W.: 1969, *Astrophys. Space Sci.* **5**, 113.
Feenberg, E. and Trigg, G.: 1950, *Revs. Mod. Phys.* **22**, 399.
Garvey, G. T. and Kelson, I.: 1966, *Phys. Rev. Letters* **16**, 197.
Greenstein, J. L.: 1968, private communication.
Hansen, C. J.: 1966, Ph.D. Thesis, Yale University (unpublished).
Hansen, C. J.: 1968, *Astrophys. Space Science* **1**, 499.
Landau, L. D. and Lifshitz, E. M.: 1958, *Statistical Physics*, Addison-Wesley Publishing Co., Reading, Mass.
Mestel, L. and Ruderman, M. A.: 1967, *Monthly Notices Roy. Astron. Soc.* **136**, 27.
Tsuruta, S.: 1964, Ph.D. Thesis, Columbia University (unpublished).
Tsuruta, S. and Cameron, A. G. W.: 1965, *Can. J. Phys.* **43**, 2056.
Van Horn, H. M.: 1968, *Astrophys. J.* **151**, 227.